Voltammetry under Microfluidic Control: Computer-Aided Design Development and Application of Novel Microelectrochemical Reactors

I. E. Henley, K. Yunus, and Adrian C. Fisher*

Department of Chemistry, University of Bath, Claverton Down, Bath BA2 7AY, United Kingdom

Received: December 6, 2002; In Final Form: January 29, 2003

We describe the development, numerical quantification, and application of a new class of microelectrochemical reactors (MECR). The reactors were fabricated using standard photolithographic techniques and a photosensitive propriety glass to yield structurally well-defined rectangular ducts of the following critical dimensions: height 25−100 μm, width 100−500 μm, and length 1−10 cm. Separate microelectrode sensors were constructed on a base plate, and the two components were bonded to yield the MECR. Finite element (FE) simulations were carried out to aid in the design and quantification of the voltammetric analysis performed using the new devices. The numerical results revealed the 3D fluid dynamic and mass transport behavior within these cells and were used to quantify the variation of the 3D current density at the working electrode as a function of the transport rate through the cell. Experimental MECR studies were undertaken using aqueous and organic solutions containing ferrocene and potassium ferrocyanide to establish the experimental variation of the electrolysis current as a function of the solution flow rate. In both the numerical and experimental cases, a well-defined relationship between the mass-transport-limited current and volume flow rate was observed, and quantitative agreement between theory experiment was obtained for all cases explored.

Introduction

Hydrodynamic voltammetry has become a well-established and powerful technique for a wide variety of applications including continuous chemical monitoring, high-throughput screening, and the mechanistic analysis of electrolysis processes.[1−3] One popular approach has exploited the channel electrode flow cell, where a working electrode is placed smoothly into the wall of a rectangular duct and electrolyte solution is pumped through the cell under laminar flow conditions. By careful design of the device, well-defined mass-transport conditions prevail, and quantitative analysis may then be performed by an examination of the current/transport-rate response of a specific system. The application of channel electrodes has been illustrated in many systems (e.g., following chromatographic separations[4,5] and in combination with spectroelectrochemical studies such as IR, UV/vis, ESR, and fluorescence spectroscopy[6−9]). Concepts such as photoelectrochemical processes have also been explored with the use of channel electrodes,[10−16] and more recently, we have demonstrated voltammetric analysis in immiscible multiphase processes.[17−19]

In parallel with the application of hydrodynamic electrochemical techniques in recent years, there have been rapid developments in the application of microscale reactors with dimensions on the order of 100 μm.[20−25] These have already been exploited in an enormous range of fields including biochemical analysis, chemical synthesis, multiphase flow, and high-throughput screening.

Recently, we have sought to combine the merits of traditional hydrodynamic voltammetric techniques with microreactor technology, and we demonstrated qualitatively the merits of combining these microscale reactors with electrochemical-based sensing.[26−28] In particular, we have adopted a cell fabrication strategy that permits structurally precise and well-defined glass rectangular ducts to be fabricated (a schematic of a typical MECR is shown in Figure 1), and in this article, we significantly extend our previous studies to permit quantitative voltammetric analysis using MECR to be performed. Specifically, we outline the application of 3D finite element techniques to quantify the variation of the transport-limited current as a function of transport rate through the cell. This approach develops previous work presented by the group for devices that may be examined using 2D electrolysis analysis under both stagnant and fluid-flow conditions.[29−35]

In this article, we examine the response of a range of MECR devices with varying dimensions and use the finite element method to calculate the transport-limited current as a function of the volume flow rate. Experimental investigations are also reported; the results are compared with those predicted numerically, and excellent agreement is observed.

Theory

Governing Equations. In this section, we develop a model of the mass transport and electrolysis reactions occurring within the cell shown in Figure 1. The cell consists of a rectangular duct constructed of a channel unit and an electrode cover plate sandwiched together to form a microelectrochemical reactor. In this paper, we consider the transport-limited one-electron reduction of A

$$A + e^-_{(m)} \rightarrow B$$

at the working electrode where sufficient electrolyte has been added to the solution to permit the neglect of any migratory

* Corresponding author. E-mail: chsacf@bath.ac.uk. Fax: 44-1225-826231.

10.1021/jp022533v CCC: $25.00
Published on Web 04/01/2003

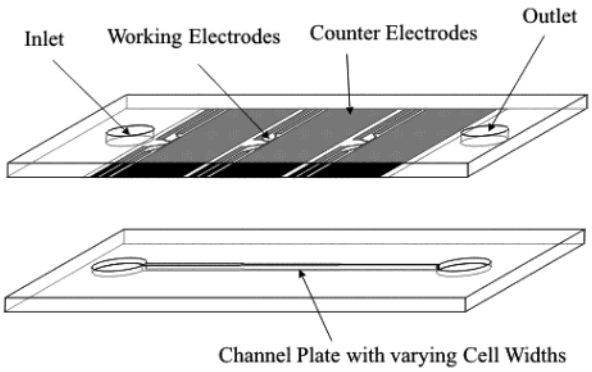

Figure 1. Schematic of a typical microelectrochemical reactor.

transport. The 3D mass transport equation of interest is then given by

$$D\frac{d^2C}{dx^2}+D\frac{d^2C}{dy^2}+D\frac{d^2C}{dz^2}+u\frac{dC}{dx}+v\frac{dC}{dy}+w\frac{dC}{dz}=0 \quad (1)$$

where C is the concentration of a species, D is the diffusion coefficient, and u, v, and w are the velocities of the solution in the x, y, and z directions, respectively. To calculate the concentration distribution within the cell from eq 1, it is first necessary to solve the relevant fluid dynamic equations and determine u, v, and w. In this article, it is assumed that the fluid is Newtonian and incompressible in behavior, so the steady-state Navier−Stokes equations are solved (eqs 2−4)[36,37] simultaneously with the continuity equation (eq 5) subject to appropriate boundary conditions by application of the finite element method.

$$\rho\left(\frac{du}{dt}+u\frac{du}{dx}+v\frac{du}{dy}+w\frac{du}{dz}\right)= -\frac{dp}{dx}-\mu\left(\frac{d^2u}{dx^2}+\frac{d^2u}{dy^2}+\frac{d^2u}{dz^2}\right) \quad (2)$$

$$\rho\left(\frac{dv}{dt}+u\frac{dv}{dx}+v\frac{dv}{dy}+w\frac{dv}{dz}\right)= -\frac{dp}{dy}-\mu\left(\frac{d^2v}{dx^2}+\frac{d^2v}{dy^2}+\frac{d^2v}{dz^2}\right) \quad (3)$$

$$\rho\left(\frac{dw}{dt}+u\frac{dw}{dx}+v\frac{dw}{dy}+w\frac{dw}{dz}\right)= -\frac{dp}{dz}-\mu\left(\frac{d^2w}{dx^2}+\frac{d^2w}{dy^2}+\frac{d^2w}{dz^2}\right) \quad (4)$$

$$\frac{du}{dx}+\frac{dv}{dy}+\frac{dw}{dz}=0 \quad (5)$$

where p is the pressure, ρ is the density, and μ is the viscosity.

Finite Element Method

Using the finite element method, the domain of interest is divided into an interconnecting mesh of elements, and in this paper, a fully 3D approach is presented where both the convection and diffusion are calculated for the whole 3D space using a well-documented hexahedral-shaped element with 20 nodes[36,38−40] (Figure 2) for the fluid dynamics and 8 nodes for the convective-diffusion. The values of the primitive variables are defined at the node points and interpolated throughout the rest of the element using an interpolation function derived from

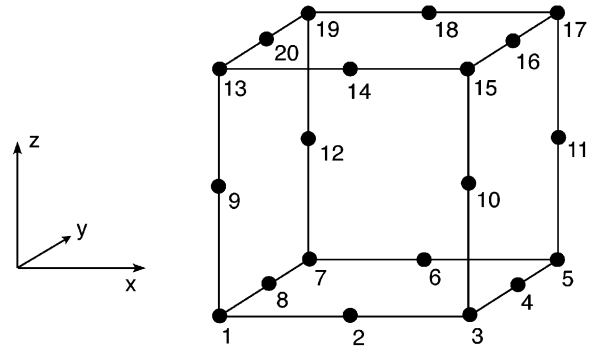

Figure 2. Twenty-node hexehedral element.

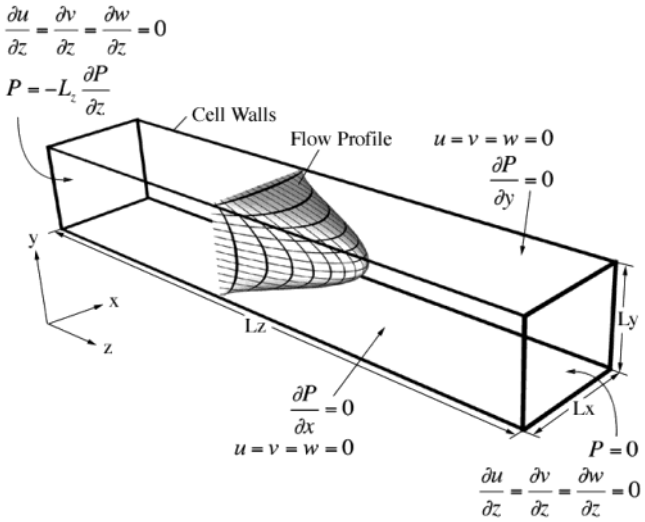

Figure 3. Boundary conditions for fluid dynamics in a channel.

TABLE 1: Boundary Conditions for Fluid Dynamic Simulation

boundary	u	v	w	P
$z=0$	$\frac{\partial u}{\partial z}=0$	$\frac{\partial v}{\partial z}=0$	$\frac{\partial w}{\partial z}=0$	$P=-Lz\frac{\partial P}{\partial z}$
$z=Lz$	$\frac{\partial u}{\partial z}=0$	$\frac{\partial v}{\partial z}=0$	$\frac{\partial w}{\partial z}=0$	$P=0$
$x=0$	$u=0$	$v=0$	$w=0$	$\frac{\partial P}{\partial x}=0$
$x=Lx$	$\frac{\partial u}{\partial z}=0$	$\frac{\partial v}{\partial z}=0$	$\frac{\partial w}{\partial z}=0$	$\frac{\partial P}{\partial x}=0$
$y=0$	$u=0$	$v=0$	$w=0$	$\frac{\partial P}{\partial y}=0$
$y=Ly$	$u=0$	$v=0$	$w=0$	$\frac{\partial P}{\partial y}=0$

the appropriate polynomial basis set. Equation 6 shows the polynomial basis for the 20-noded element.

$$\langle P\rangle = \left\langle 1 \quad x \quad y \quad z \quad x^2 \quad xy \quad y^2 \quad yz \quad z^2 \quad xz \quad x^2y \quad xy^2 \quad y^2z \quad yz^2 \quad xz^2 \quad x^2z \quad xyz \quad x^2yz \quad xy^2z \quad xyz^2 \right\rangle \quad (6)$$

Solutions of the convective diffusion and Navier−Stokes equations were performed using the Galerkin residual method[41] that we have previously employed successfully for 2D electrochemical simulations. The boundary conditions employed for the fluid dynamic calculations are shown in Figure 3 and Table 1.

A typical grid for a fluid dynamic calculation would contain on the order of four elements in the direction of flow and eight

elements in the other two directions. The grid was exponentially expanded from the walls of the channel in the *y* and *z* directions with a first element size of 5 μm such that the smallest elements were at the edge and large elements were in the middle.

To solve the convective diffusion (eq 1), an expanding grid in the *z* direction was used from the edges of the electrode to the center of the electrode and from the edges of the electrode to the ends of the grid.[42,35] This was needed to model the rapid changes in concentration that occur at the edges of the diffusion layer as a result of thinning with high convection. The grid was also expanded from the surface of the electrode up to the channel wall opposite for the same reason. The first element sizes were varied according to the amount of convection added and were on the order 0.1 μm in length. A typical number of elements used was $20 \times 20 \times 90$ in the *x*, *y*, and *z* directions, respectively. This resulted in a grid with an order of 40 000 nodes and thus the same number of simultaneous equations to be solved. A frontal-based code was found to be effective in solving the matrix equations.[36] The current was evaluated numerically using

$$i = -nFDAJ \tag{7}$$

where *i* is the current, *n* is the number of electrons transferred per reaction, *F* is the Faraday constant, *D* is the diffusion coefficient, *A* is the electrode area, and *J* is the concentration flux at the surface of the electrode. *J* was determined by numerically integrating the derivative of the interpolation function with respect to *y* at the electrode surface for all of the elements that lie on the electrode.

Experimental Section

The MECR devices were fabricated as reported previously,[43,44] and a practical design is shown in Figure 1. Rectangular ducts were etched into Foturan glass plates to yield a range of channel dimensions: height 40−100 μm, width 100−500 μm, and length 1−3 cm. The method of sealing the glass cover plate was modified from the previously reported wax approach to a clamping scheme for the thinnest cells.[45] Chrome/gold films were evaporated (Emitech Evaporator, model K975) onto the glass cover plate using standard photolithographic procedures,[46] and a range of microband electrode lengths were fabricated: 20−100 μm. A typical image of a set of microband electrodes is shown in Figure 8. All of the microband electrodes were positioned in the MECR devices after a lead-in length from the inlet to establish poiseuille flow.[47]

The solvent employed in these studies was acetonitrile (Aldrich, 99.93+% HPLC grade). *N*,*N*,*N*′,*N*′-Tetramethyl-1,4-phenylene diamine (TMPD) (Aldrich, 98%) was used as received, and tetrabutylammonium perchlorate (TBAP) (Fluka, 99.9%) acted as the background electrolyte. In all cases, the solutions were degassed with predried nitrogen[48] for 15 min before flowing under gravity[30,49] through the MECR devices. Voltammetric measurements at the microband electrodes were carried out using an ECO CHEMI PGSTAT 100.

All numerical simulations were written in C++ and were run on a Compaq Alpha XP1000 workstation. Typical run times ranged between 3 and 45 min depending upon the conditions employed.

Results and Discussion

Preliminary calculations were performed to evaluate the validity and accuracy of the developed codes. First, the fluid dynamic calculations were performed for a simulation of the flow within a thin, wide channel (resulting in a parabolic flow profile in the *z* direction), and the results were compared to those predicted analytically. The cell geometry was $Ly = 100$ μm (height) and $Lx = 1000$ μm (width). Excellent agreement with analytical results was observed (Figure 4).

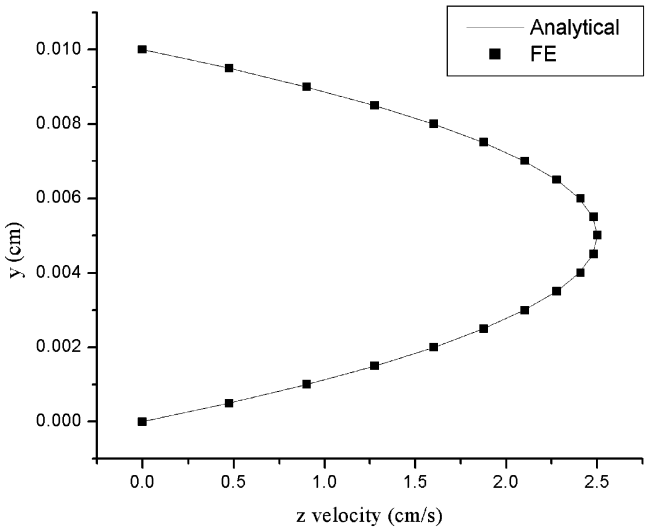

Figure 4. Velocity profile in a 1000 μm × 100 μm channel.

Next, the mass transport code was tested using a similar strategy to that described above. The variation of the current flow at a microband electrode sited within a thin but infinitely wide duct was examined. The height of the cell (*Ly*) was 100 μm with an electrode of length 20 μm. A "no-flux" boundary condition was applied on the boundaries at $x = 0$ and *Lx* in both the fluid dynamic and concentration calculations for all variables, thus assuming an infinitely wide cell. In this case, the current density across the electrode (*x* direction) should be invariant with distance, and this was observed for all of the simulated cases. In addition, at sufficiently high flow rates where axial diffusion from the microelectrode may be neglected, the variation of the transport-limited current as a function of the volume flow rate (V_{fr}) should follow that predicted analytically;[32] again, excellent agreement was observed between the numerical model and the analytical predictions.

Having established the validity of the new codes, full 3D current flow-rate simulations were undertaken for a range of different MECR geometries, and the results below are presented for the flow-cell geometries $Lx = 500$, 240, and 120 μm (width) and $Ly = 100$ μm (height). Microband electrodes were sited across the whole width of the cell, with lengths of 100, 60, and 20 μm, and a mass-transport-limited one-electron reduction was driven at the working microband electrode. The viscosity and density were used for water, and a diffusion coefficient of 1×10^{-5} cm^2 s^{-1} was used for the electroactive reagent. Current density calculations were performed for each different geometry to explore the influence of the current "edge effect"[3] caused by the hydrodynamic boundary layer at the cell wall. Figure 5a−c shows plots of the normalized current density integrated across the working electrode where *I* is current per cm and I_c is the maximum current density in the center of the channel. A typical velocity profile for the 240-μm cell can be seen in Figure 6. In all of the cases addressed (V_{fr} in the range of 1×10^{-5} to 1×10^{-2} cm^3/s), the current density can be seen to drop in regions close to the side wall because of the hydrodynamic boundary layer, with the effect most significant for the narrow cell. Next, the mass-transport-limited current/flow-rate behavior was examined to obtain a quantitative model of the voltammetric response anticipated for the following experimental measure-

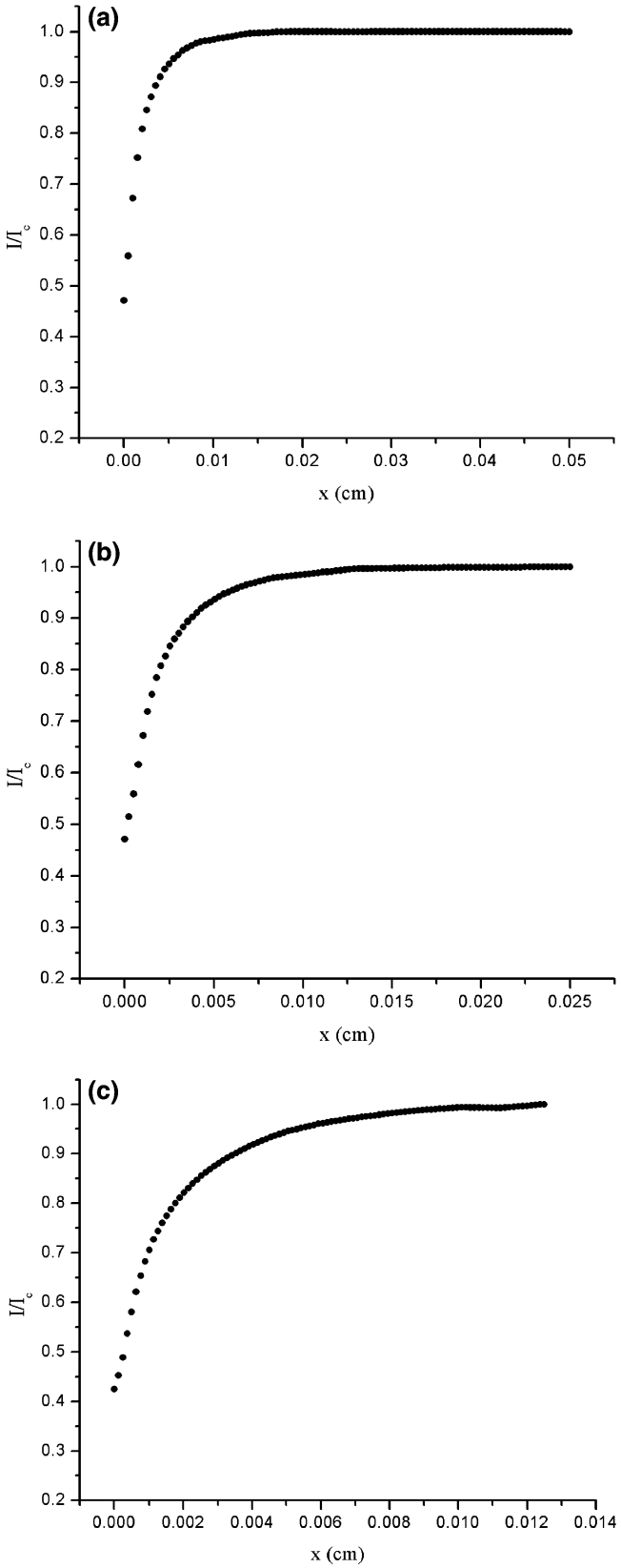

Figure 5. Typical current-density plots across the electrode in (a) 1000-μm-wide, (b) 500-μm-wide, and (c) 250-μm-wide channels with volume flow rates of 2.6×10^{-3}, 1.2×10^{-3}, and 5.0×10^{-3} cm^3/s, respectively.

ments. Figure 7 shows the variation of the transport-limited current as a function of the cube root of the volume flow rate ($V_{fr}^{1/3}$) for each of the cell configurations identified above with a 20-μm electrode using volume flow rates in the range of 0.0001 to 0.01 cm^3/s. In each case, a linear relationship between

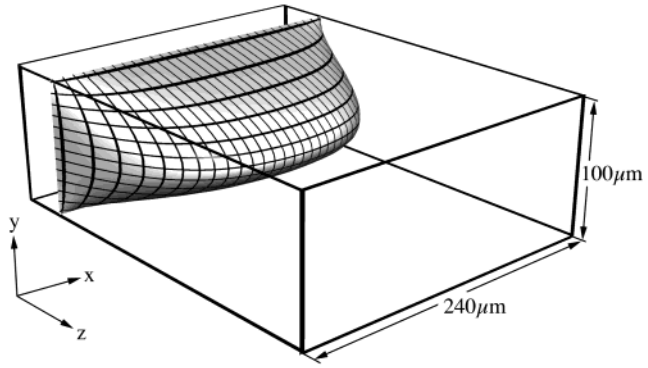

Figure 6. Velocity profile in a microcell of dimensions 240 μm $\times$ 100 μm.

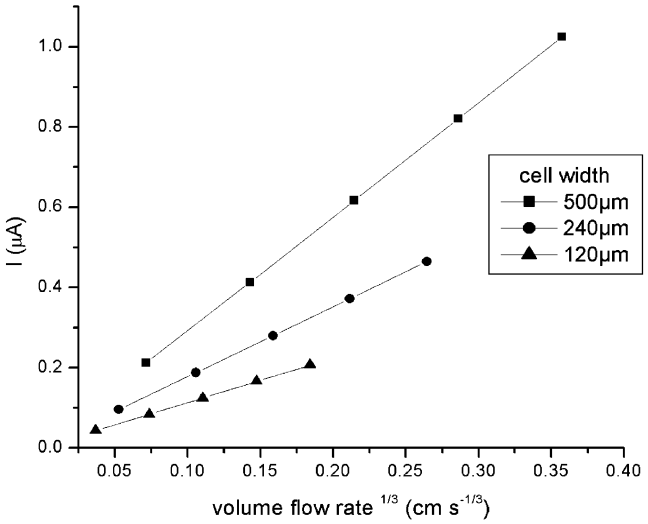

Figure 7. Current−flow-rate simulations for a 20-μm-channel electrode with a cell height of 100 μm.

I_{lim} and $V_{fr}^{1/3}$ was observed, in an analogous manner to that observed for macroscopic channel flow-cell measurements where the channel width is assumed to be infinite to permit a simplified 2D analysis approach. It is interesting that this approach remains valid for the microelectrochemical reactors employed in these studies despite the influence of the hydrodynamic boundary layer close to the far walls of the cell.

Having examined the numerical predictions, experimental measurements were then undertaken to examine whether the proposed models provide a quantitative description of the measurements that were performed.

Experiments were performed using the oxidation of TMPD, which is well known to undergo a reversible one-electron transfer,[50] in acetonitrile solution containing 0.1 M TBPA. The analysis focused on examining the quantitative relationship between the transport-limited current as a function of volume flow in MECR devices.

Initial measurements were carried out to quantify the response observed for a microband electrode in an MECR device under no-flow conditions. A solution of acetonitrile containing 1.126×10^{-3} M TMPD and 0.1 M TBAP background electrolyte was prepared. A series of linear sweep voltammograms were conducted at various scan rates ranging between 5 and 500 mV/s using two different microbands of lengths 20 and 40 μm. Figure 9 shows the typical response observed for a cell of width 500 μm, height 100 μm, and length 2 cm using a microband of length 20 μm and width 500 μm. For a stagnant system, the variation of the peak current density (I_p) as a function of the dimensionless

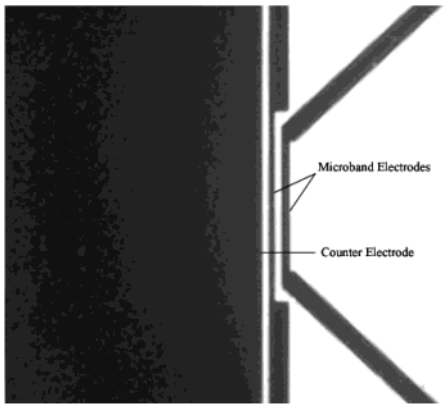

Figure 8. Typical image of two fabricated microband electrodes.

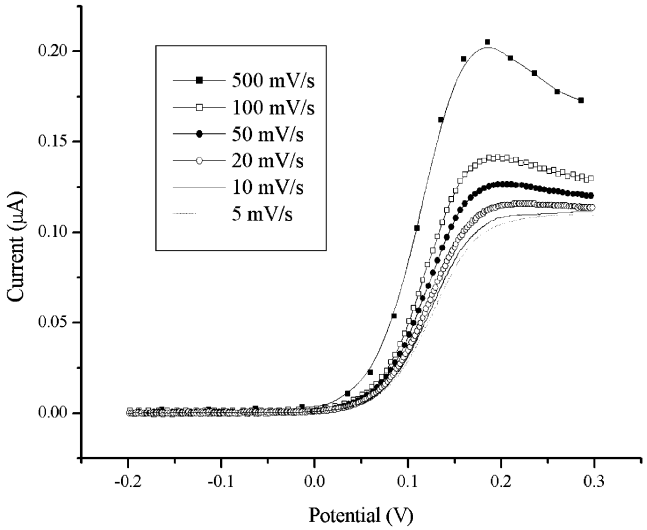

Figure 9. Voltammetric response of microband electrodes in a microelectrochemical reactor. Typical data recorded for a 20-μm microband electrode at varying voltage scan rates using a solution of acetonitrile containing 1.126×10^{-3} M TMPD and 0.1 M TBAP as background electrolyte.

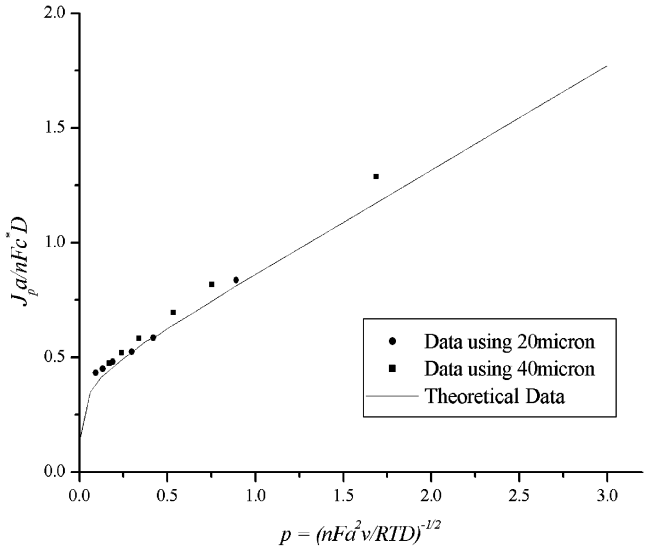

Figure 10. Dimensionless analysis of peak current density against voltage scan rate.

voltage scan rate (p) should obey the analytical response predicted for a microband electrode.[51] Figure 10 describes the dimensionless analysis, and good agreement can be seen between the values predicted and those recorded experimentally.

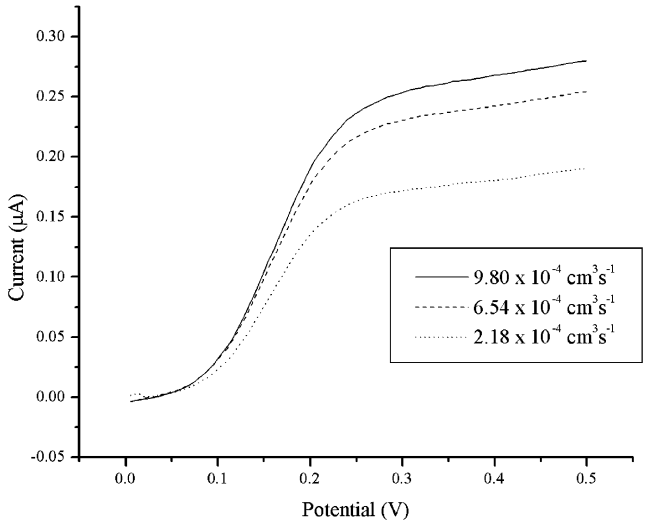

Figure 11. Steady-state voltammograms recorded for a 0.472 mmol TMPD solution at different flow rates for an MECR with the following dimensions: height 40 μm, width 100 μm, and length 3 cm. The microband used in this measurement had the dimensions: length 50 μm and width 100 μm.

Having established the optimum response for MECR devices under stagnant conditions, experiments were conducted to interrogate the behavior of the devices under steady-flow conditions. The electrolysis reaction of TMPD in acetonitrile was studied with a range of microband electrodes and was used to study the relationship between the variation of the transport-limited current as a function of V_{fr}. Figure 11 shows typical steady-state voltammograms recorded at a scan rate of 10 mV/s for a microband electrode of length 50 μm and width 100 μm. The MECR had the following dimensions: height 40 μm, width 100 μm, and length 3 cm. The volume flow rates that were used were in the range of 1×10^{-4} to 1×10^{-3} cm^3 s^{-1}, and the solution contained 0.472 mmol of TMPD and 0.1 M TBAP as a background electrolyte. It can be seen that the transport-limited current depends strongly on the transport rate through the cell, and this behavior is analogous to that observed in the simulated results shown in Figure 7 as well as to that reported for macroscopic channel electrodes.[49,52]

A series of voltammetric measurements were conducted using a wide range of MECR dimensions to determine and quantify the variation of transport-limited current as a function of V_{fr}. Figures 12 and 13 reveal a typical set of data recorded for two different MECR devices. The data shown in Figure 13 was obtained by using a microband electrode of length 35 μm and an MECR device with the following dimensions: height 40 μm, width 100 μm, and length 3 cm. In the case of Figure 13, the analysis was carried out using a microband electrode of length 27.5 μm, and the MECR device had the following dimensions: height 40 μm, width 200 μm, and length 3 cm. In all of the measurements, linear sweep voltammograms were recorded at a voltage scan rate of 10 mV/s to establish the transport-limited current at varying V_{fr}. Both devices show a variation of the transport-limited current as a function of $V_{fr}^{1/3}$, and in both configurations, the transport-limited current is seen to be proportional to $V_{fr}^{1/3}$. The relationship of the transport-limited current to the concentration of TMPD solution is also illustrated in the Figures and is shown to be proportional as expected. This was observed for all of the different MECR dimensions for a range of microband lengths.

The results shown in Figures 12 and 13 have been overlaid with the simulated results to show good agreement. It is

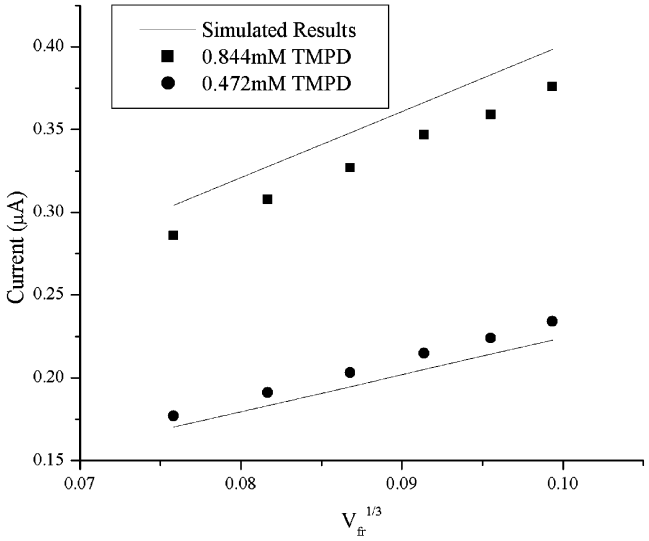

Figure 12. Experimental and theoretical behavior for the transport-limited current as a function of flow rate in a MECR of dimensions: height 40 μm, width 100 μm and length 3 cm. The microband electrode used in this measurement had the dimensions: length 35 μm and width 100 μm.

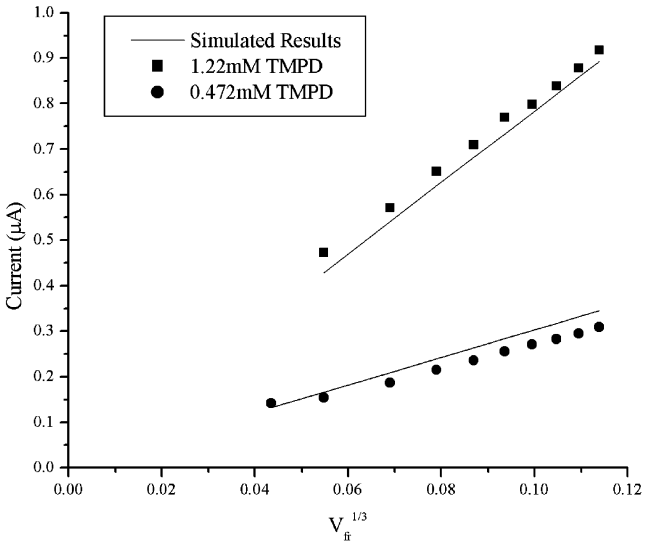

Figure 13. Experimental and theoretical behavior for the transport-limited current as a function of flow rate in an MECR with the following dimensions: height 40 μm, width 200 μm, and length 3 cm. The microband electrode used in this measurement had the following dimensions: length 27.5 μm and width 200 μm.

interesting that the observed response is in accordance with levich analysis.[52] Even though the electrode is stretched across the whole width of the device, a response due to edge effects is not noticed as predicted by the simulations.

Conclusions

Three-dimensional fluid dynamic and convective-diffusion FEM codes have been shown to be effective at predicting the mass transport and currents in electrochemical flow cells and are stable at experimentally accessible flow rates. The current against $V_{fr}^{1/3}$ behavior for a microchannel approaching a square cross section is shown to agree with levich analysis despite the influence of an edge effect near the channel walls. This is shown to be due to the insignificant amount of sideways diffusion of species as a result of the high fluid velocities used experimentally.

A novel approach to fabricating well-defined microelectrochemical reactors has also been illustrated. It has been shown that the MECR design gives an optimum response for the device and that this has been proven by demonstrating good agreement with that predicted by the finite element method.

References and Notes

(1) Brett, C. M. A. *Comput. Chem. Kinet.* **1999**, *37*, 573.
(2) Brett, C. M. A.; Maria, A. *Comput. Chem. Kinet.* **1986**, *26*, 355.
(3) Cooper, J. A.; Compton, R. G. *Electroanalysis* **1998**, *10*, 141−155.
(4) Kissinger, P. T. *Anal. Chem.* **1997**, *499*, 447A−456A.
(5) Wightman, R. M.; Paik, E. C.; Borman, S.; Dayton, M. A. *Anal. Chem.* **1978**, *50*, 1410−1414.
(6) Kastening, B. *Anal. Chem.* **1967**, *39*, 224.
(7) Dohrmann, J. K.; Galluser, F.; Wittchen, H. *Faraday Discuss. Chem. Soc.* **1973**, *56*, 350.
(8) Webster, R. D.; Dryfe, R. A. W.; Eklund, J. C.; Lee, C. W.; Compton, R. G. *Electroanal. Chem.* **1996**, *167*, 402.
(9) Compton, R. G.; Coles, B. A.; Pilkington, M. B. G.; Bethell, D. J. *J. Chem. Soc., Faraday Trans.* **1990**, *86*, 663.
(10) Dryfe, R. A. W.; Compton, R. G. *Prog. React. Kinet.* **1995**, *20*, 245.
(11) Fisher, A. C.; Compton, R. G.; Coles, B. A.; Bethell, D. J.; Tripathi, S. J. *J. Chem. Soc., Faraday Trans.* **1990**, *86*, 3603.
(12) Compton, R. G.; Eklund, J. C.; Fisher, A. C.; Waller, A. M. *J. Chem. Soc., Faraday Trans.* **1990**, *86*, 2951.
(13) Compton, R. G.; Fisher, A. C.; Wellington, R. G.; Bethell, D.; Lederer, P. *J. Phys. Chem.* **1991**, *95*, 4749−4752.
(14) Compton, R. G.; Fisher, A. C.; Wellington, R. G.; Bethell, D. *Port. Electrochim. Acta* **1991**, *9*, 271.
(15) Compton, R. G.; Dryfe, R. A. W.; Fisher, A. C. *J. Electroanal. Chem.* **1993**, *361*, 275−278.
(16) Compton, R. G.; Dryfe, R. A. W.; Eklund, J. C.; Hirst, J.; Nei, L.; Fleet, G. W. J.; Hsua, K. Y.; Bethell, D.; Martingale, L. J. *J. Chem. Soc., Perkin Trans. 2* **1995**, *8*, 1973.
(17) Fisher, A. C.; Gooch, K. A.; Yunus, K.; Allsopp, D. W. E.; Ryan, T. J. International Symposium on the Chemical Characterization of Liquid|Liquid and Liquid|Membrane Interfaces for the Development of Novel Reaction Fields, Kyoto, Japan, 2001.
(18) Yunus, K.; Marks, C. B.; Fisher, A. C.; Allsopp, D. W. E.; Ryan, T. J.; Dryfe, R. A. W.; Hill, S. S.; Roberts, E. P. L.; Brennan, C. M. *Electrochem. Commun.* **2002**, *4*, 579−583.
(19) Fisher, A. C.; Yunus, K.; Henley, I. E.; Dryfe, R. A. W.; Hill, S. S. *Anal. Chem.*, submitted for publication.
(20) Fisher, A. C.; Gooch, K. A.; Henley, I. E.; Yunus, K. *Anal. Sci.* **2001**, *17*, i371−i374.
(21) Ismagilov, R. F.; Kenis, P. J. A.; Stroock, A. D.; McDonald, J. C.; Stone, H. A.; Whitesides, G. M. *Abstr. Pap.−Am. Chem. Soc.* **1999**, *218*, 247-ORGN.
(22) Manz, A.; Eijkel, J. C. T. *Pure Appl. Chem.* **2001**, *73*, 1555−1561.
(23) Qin, D.; Xia, Y. N.; Rogers, J. A.; Jackman, R. J.; Zhao, X. M.; Whitesides, G. M. *Microsyst. Technol. Chem. Life Sci.* **1998**, *194*, 1−20.
(24) Whitesides, G. M.; Stroock, A. D. *Phys. Today* **2001**, *54*, 42−48.
(25) Xia, Y. N.; Whitesides, G. M. *Angew. Chem., Int. Ed.* **1998**, *37*, 551−575.
(26) Naz, A.; Effenhauser, C. S.; Barggraf, N.; Verpoorte, E. J. M.; Raymond, D. E.; Widmer, H. M. *Analusis* **1994**, *M25*, 22.
(27) Ehrfeld, W.; Gratner, C.; Hessel, R. K.; Lowe, H. T. R.; Schulz, C. *Fabrication of Components and Systems for Chemical Biochemical Microreactors* Springer: Berlin, 1998.
(28) Jackel, K. P. *Microtechnology* **1996**, *29*, 132.
(29) Qiu, F. L.; Gooch, K. A.; Fisher, A. C.; Stevens, N. P. C.; Compton, R. G. *Anal. Chem.* **2000**, *72*, 3480−3485.
(30) Qiu, F. L.; Stevens, N. P. C.; Fisher, A. C. *J. Phys. Chem. B* **1998**, *102*, 3779−3783.
(31) Qiu, F. L.; Williams, N. A.; Fisher, A. C. *Electrochem. Commun.* **1999**, *1*, 124−127.
(32) Stevens, N. P. C.; Fisher, A. C. *J. Phys. Chem. B* **1997**, *101*, 8259−8263.
(33) Stevens, N. P. C.; Fisher, A. C. *Electroanalysis* **1998**, *10*, 16−20.
(34) Stevens, N. P. C.; Gooch, K. A.; Fisher, A. C. *J. Phys. Chem. B* **2000**, *104*, 1241−1248.
(35) Gooch, K. A.; Williams, N. A.; Fisher, A. C. *Electrochem. Commun.* **2000**, *2*, 51−55.
(36) Taylor, C.; Hughes, T. G. Pineride Press: 1981.
(37) Geankoplis, C. J. Allyn and Bacon Inc., 1983.
(38) Dhat, G.; Touzot, G.,; Wiley-Interscience: 1984.
(39) Zeinkiewicz, O. C.; Taylor, R. L. McGraw-Hill: London, 1991.
(40) Cuvelier, S.; Segal, A.; van Steenhoven, A. ReidelDordrecht: Holland, 1986.

(41) Rao, S. S.,; Pergamon Press: Oxford, U.K., 1982.
(42) Nann, T.; Heinze, J. *Electrochem. Commun.* **1999**, *1*, 289−294.
(43) Yunus, K.; Fisher, A. C. *Electroanalysis*, in press.
(44) Fisher, A. C.; Gooch, K. A.; Henley, I. E.; Yunus, K. *Anal. Sci.* **2001**, *17*, i371.
(45) Brown, C. A.; Compton, R. G.; Narramore, C. A. *J. Colloid Interface Sci.* **1993**, *160*, 372−379.
(46) Dietrich, T. R.; Ehrfeld, W.; Lacher, M.; Krmer, M.; Speit, B. *Microelectron. Eng.* **1996**, *30*, 497.
(47) Schlichting, H. Pergamon Press: London, 1995.
(48) Meschi, P. L.; Johnson, D. C. *Anal. Chem.* **1980**, *52*, 1304−1308.
(49) Compton, R. G.; Fisher, A. C.; Wellington, R. G.; Dobson, P. J.; Leigh, P. A. *J. Phys. Chem.* **1993**, *97*, 10410−10415.
(50) Moressi, M. B.; Fernndez, H. *J. Electroanal. Chem.* **1994**, *153*, 369.
(51) Aoki, K. *Electroanalysis* **1993**, *5*, 627−639.
(52) Levich, B. *Physicochemical Hydrodynamics*, 2nd ed.; Prentice Hall: Englewood Cliffs, NJ, 1962.